Nanofabrication (2022) 7, 89-103
https://doi.org/10.37819/nanofab.007.212

eurasia

RESEARCH ARTICLE

Check for updates

Investigation of Ag doping and ligand engineering on green synthesized CdS quantum dots for tuning their optical properties

Narendra Singh,[a,b] Shivam Prajapati,[a] Prateek,[a] and Raju Kumar Gupta*[a,c,d]

[a]*Department of Chemical Engineering, Indian Institute of Technology Kanpur, Kanpur-208016, UP, India*
[b]*Department of Chemical Engineering, Indian Institute of Technology Tirupati, Tirupati, Andhra Pradesh, 517506, India*
[c]*Center for Environmental Science and Engineering, Indian Institute of Technology Kanpur, Kanpur-208016, UP, India*
[d]*Department of Sustainable Energy Engineering, Indian Institute of Technology Kanpur, Kanpur-208016, UP, India*
**Corresponding author email: guptark@iitk.ac.in*; Tel: +91-5122596972; Fax: +91-5122590104.

ABSTRACT

We present a green route for the colloidal synthesis of undoped and silver (Ag) doped cadmium sulfide (CdS) quantum dots (QDs). We have used olive oil as the reaction medium, which acted as a source of oleic acid (OA) ligand in the green synthesis of CdS QDs. With the increase in OA concentration, the dispersibility of CdS QDs improved. The water-dispersible CdS QDs were prepared via exchanging OA's associated ligand with 3-mercaptopropionic acid (MPA). The MPA-capped CdS QDs showed the disappearance of the S-H peak as characterized via FTIR. The crystal and optical properties of Ag-doped CdS QDs were investigated, and the spectral red shift in the absorption spectra was observed. The CdS QDs with low Ag doping concentration increased the lifetime of excitons, but the average lifetime was suppressed at a higher concentration. We also discussed the variation in the properties of the CdS QDs through the ligand engineering and Ag doping. These doped and undoped QDs have the potential for applications in photocatalysis, water splitting, solar cells, etc. In addition, water dispersible QDs can be helpful for bioimaging, and drug delivery applications.

ARTICLE HISTORY

Received: 9-03-2022
Revised: 2-07-2022
Accepted: 12-07-2022

KEYWORDS

Quantum dots;
Green synthesis;
Ag doping;
Water dispersible quantum dots;
Ligand engineering

1 Introduction

Materials properties (e.g. metal nanoparticles, QDs, graphene, etc.) can be tuned with the variation in shape and structure, which can be very useful in biosensing, energy, and drug delivery [1-3]. So QDs have attracted significant interest because of their tunable optical and electrical properties with size from the quantization effect. These have potential applications in the various fields of solar cell, laser, drug delivery, photocatalysis, photodetectors, light emitters, and bioimaging [2-6]. Generally, the QDs have been prepared by solution methods. These include long-chain capping agents/solvents, including tri-n-octyl phosphine oxide, polyethyleneimine trioctylphosphine, and tributylphosphine, which are toxic so the need for alternate environment-friendly route [7-8]. Recently, the synthesis of QDs using a greener route is receiving greater attention

because of the reduced environmental impact, waste production, process safety, minimization of chemical hazards to health, and energy efficiency [5,9-10]. Furthermore, nanostructures' synthesis without auxiliary solvents leads to more environmentally friendly nanomaterials with low toxicity [11-12].

QDs are tiny nanostructures in the range of a few nanometers, which shows the variable optical property with size [13-14]. These exhibit a high surface-to-volume ratio making them highly unstable. Therefore, ligands are used to stabilize QDs in a solution. Electrostatic forces and chemisorption bonding cause this stabilization [15]. These ligands also prevent them from agglomeration by steric hindrance or electrostatic repulsion. Depending on the ligand open side, nanoparticles are hydrophobic, hydrophilic, and useful for specific applications. CdS QDs are promising due to their visible absorption property (energy bandgap of bulk material ~2.4 eV), low-cost preparation, and high molar extinction coefficient [16]. Optical properties can be harmonized with the desired application by tuning its size [17-19].

Recently, many green synthetic routes have been developed to synthesize QDs to make them environmentally friendly. Kyobe et al. synthesized the variable size CdS QDs using castor and ricinoleic acid as a capping agent. They observed the shift in the absorption and PL peaks with the variation in length [20]. Similarly, CdSe QDs were also prepared using the biobased capping agent (castor oil and ricinoleic acid) [21]. Yang and co-workers used a biosynthetic procedure to synthesise CdS nanocrystal. They used the strain of *Stenotrophomonas maltophilia* for the extracellular production of CdS nanostructure [22]. Kandasamy and co-workers synthesized the CdS QDs using fruit sap *Opuntia ficus-indica*, which was a stabilizing and capping agent. The QD's size was found in the range of 3-5 nm [23]. The Co-doped CdS QDs were successfully synthesized through a chemical route using 1-monothioglycerol as a capping agent. The optoelectronic properties can be tuned with the variation in the Co doping [24]. Ag-doped CdS nanostructure was synthesized through the co-precipitation method and found the reduction in band gap upon Ag doping in comparison to CdS QDs. Ag doped CdS QDs were prepared using the mercaptoacetic acid as a capping agent and utilized for the detection of hydrogen sulfide in the wastewater samples [25]. Thakur and co-workers synthesized Ag@CdS QDs in which Ag^+ ions were added to CdS nanostructure. They studied the effect of dopant concentration and aging on the band gap of CdS nanoparticles. Further, they explored the CdS-Ag interaction by time-resolved fluorescence, and they found that at low Ag content, the emission was enhanced, whereas, at high Ag content, the emission was quenched [26]. In this work, we synthesized the CdS QDs with variable optical properties through ligand engineering and Ag doping.

This work reports a green synthesis route to prepare Ag-doped and undoped CdS QDs. The synthesized CdS QDs were highly monodispersed in nature. We have explored the effect of OA concentration on the morphological and optical properties of QDs. Simultaneously, the ligand exchange reaction was performed to make the CdS QDs water-soluble, and a reaction mechanism was proposed. Furthermore, the effect of Ag doping on absorption, emission, surface morphology, crystal structure, and excitons lifetime has been investigated.

2 Experimental section

2.1 Materials

Cadmium oxide (CdO, 99.99%, Aldrich), olive oil (Extra Virgin), bistrimethylsilyl sulfide (TMS), oleic acid (OA, 90%, Aldrich), octadecene (99%, Aldrich), toluene (99.8%, Merck), silver nitrate ($AgNO_3$, 99%, Aldrich), 3-mercaptopropionic acid (MPA, 99% Sigma), oleylamine, 1-dodecanethiol and acetone (99.8%, Merck) were used as received without any further purification. Deionized (DI) water was used in this study.

2.2 Synthesis of CdS QDs

In the typical synthesis, 0.9375 mmol CdO, 1 mL octadecene, and OA were added in 15 mL olive oil and heated at 220 °C with continuous stirring under vacuum until CdO gets dissolved completely. In another flask, 100 µL TMS (0.45 mmol) was mixed with 2 mL olive oil and 0.5 mL of octadecene under the nitrogen atmosphere for 5-10 min. Further, the Cd solution flask was flushed with nitrogen gas, and the TMS

solution was quickly injected into the Cd solution to start the reaction. The Cd to S mole ratio in the reaction mixture was kept constant at 2:1. The temperature was maintained at 220 °C for nucleation and growth of CdS QDs. Aliquots were taken at 30 s, 2, 5, 15, and 30 min intervals with the help of a syringe and immediately injected into a centrifuge tube containing acetone for the reaction mixture's precipitation to stop the reaction. The olive oil capped QDs were separated by centrifugation for 10 min at 6500 rpm. The samples were then re-dispersed in toluene, precipitated by adding acetone, and centrifuged in the mixture solution again to collect QDs. The step was repeated three times to complete the removal of the excess olive oil. The aliquots were dried under a vacuum oven for 12 h and stored in a cold place.

To study OA concentration's effect on the CdS QDs size, we used different amounts of OA (0, 100, 500, and 1000 µL), and samples were named DS, BS, CS, and AS, respectively. The samples collected after different time intervals (30 s, 2, 5, 15 and 30 min) were named DS1, DS2, DS3, DS4, and DS5, respectively for sample DS and similar nomenclature was assigned for the BS, CS, and AS samples aliquots.

2.3 Synthesis MPA capped CdS QDs

To synthesize MPA-capped CdS QDs, 35 mg CdS QDs were dispersed in 2 mL of toluene, and then 1 mL MPA was added into the QDs solution. Further, the solution was ultrasonicated for 30 min. Then the solution was kept at room temperature for overnight, followed by centrifugation at 5000 rpm for 5 min to collect MPA-capped CdS QDs. Then MPA capped CdS QDs were washed with ethanol two times to remove the excess compounds. The resultant mixture was then vacuum dried at room temperature and stored in a cold dark place. MPA capped CdS QDs was characterized by dispersing in DI water.

2.4 Synthesis of Ag-doped CdS QDs

Ag-doped CdS QDs were prepared using a similar hot injection method for the synthesis of CdS QDs. In brief, 0.937 mmol CdO, 15 mL olive oil, 1 mL OA, and 1 mL ODE were added to a three-neck round bottom flask and heated at 220 °C under vacuum for 2 h to dissolve CdO completely. Ag stock solution was prepared in another glass vial by dissolving 13.6 mg of $AgNO_3$ in 2 mL oleylamine to make 0.04 M $AgNO_3$ solution. We prepared sulfur stock solution by adding 100 µL TMS in 0.5 mL ODE and 2 mL olive oil under nitrogen atmosphere in another flask. After CdO dissolution, the round bottom flask was redirected to the nitrogen condition to inject precursors and the preceding reaction. A mixture of 0.33 mL of Ag stock solution and 2.5 mL of 1-dodecanethiol was quickly injected into the flask immediately after the sulfur stock solution was injected. The temperature was maintained at 220 °C for nucleation and growth of QDs. Aliquots were taken at time intervals of 30 s, 2, 5, 15, and 30 min and were precipitated immediately into a centrifuge tube containing acetone. The QDs were separated *via* centrifuge at 6500 rpm for 10 min. The QDs were then re-dispersed in toluene, re-precipitated by adding acetone, and again collected *via* centrifuge. The process was repeated three times to remove the excess olive oil. The QDs were dried under a vacuum for 12 h and stored in a cold place. The schematic diagram for synthesis of OA-capped CdS, MPA capped CdS, and Ag-doped CdS QDs is shown in Fig. 1.

2.5 Characterizations

The absorption spectra of the samples were measured with a UV-Vis absorption spectrophotometer (Varian Cary 5000, Germany). The liquid samples' photoluminescence (PL) spectra were investigated using a Fluorescence Spectrophotometer (Cary Eclipse fluorescence spectrophotometer). The morphology and size of CdS and Ag doped CdS QDs were analyzed by the images taken with the Transmission electron microscope (TEM, Tecnai G^2, FEI® USA). The crystal structure of the synthesized doped and undoped CdS QDs was determined using X-ray crystallography (Rigaku MiniFlex 600, with X-ray wavelength = 0.15406 nm). Fourier transform infrared spectroscopy (FTIR) (Spectrum Two, Perkin Elmer) analysis was used to identify chemical bonds and functional groups in the materials. The surface charge of QDs was studied with Zeta potential (Malvern, Zetasizer ZS90, He-Ne red laser with 4 mW). Time-resolved photoluminescence (TRPL, FOG-100, CDP Corp., Russia) study was used to understand excitons' lifetime.

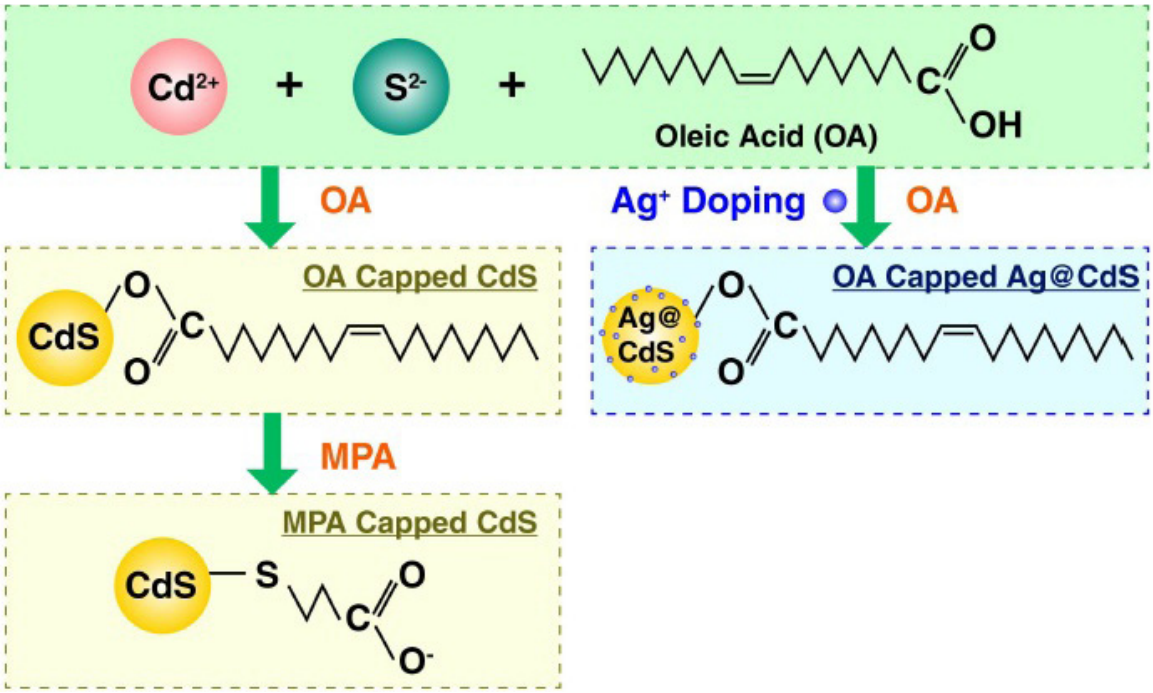

Figure 1. Schematic of synthesis of OA capped CdS, MPA capped CdS and Ag-doped CdS QDs.

3 Results and discussion

3.1 Effect of OA on optical properties of CdS QDs

OA is commonly used to prepare hydrophobic nanoparticles and as a surfactant. OA provides the nanoparticles' steric stabilization against the Van der Waals and attractive magnetic interactions, preventing agglomeration. Thus, it prevents the Ostwald ripening and hence NPs growth. Furthermore, the mass transfer of sulfur ions is restricted because of the barrier effect of the surface layer. The present study systematically examined the effect of OA concentration (used during reaction) on the optical properties of CdS QDs. Fig. 2(a) shows the absorption spectra of CdS QDs without OA's addition during the reaction. The absorption peaks were observed at 399, 403, 407, 416, and 417 nm corresponding to the different aliquots samples DS1, DS2, DS3, DS4, and DS5, respectively. The sharp absorption edges of CdS QDs of different aliquots confirm the narrow size distribution. The diameters (D, nm) of CdS QDs were calculated using the absorption data from equation 1 as given below.

$$D\ (nm) = (-6.6521 \times 10^{-8})\lambda^3 + (1.9557 \times 10^{-4})\lambda^2 - (9.2352 \times 10^{-2})\lambda + 13.29 \quad [1]$$

where λ (nm) is the wavelength of the corresponding sample's first excitonic absorption peak [27]. The calculated nanoparticle sizes were 3.35, 3.48, 3.61, 3.92, and 3.96 nm (using equation 1) for the samples DS1, DS2, DS3, DS4, and DS5, respectively. It has been observed that with increasing synthesis time, QDs gradually grow to reach the maximum average size of 3.96 nm after 30 min of synthesis.

Fig. 2(b) shows UV-Vis absorption spectra of CdS QDs prepared under the same reaction conditions with 1000 µL OA. The samples AS1, AS2, AS3, AS4, and AS5 showed the corresponding absorption peaks at 404, 406, 410, 418, and 424 nm, respectively. The calculated size of QDs was found to be 3.51, 3.58, 3.72, 4.0, and 4.22 nm, respectively, using equation 1.

Fig. 2(c) shows the absorption spectra of CdS QDs with 500 µL of OA used, and other conditions remain the same. The samples BS1, BS2, BS3, BS4, and BS5 showed absorption peaks at 401, 406, 412, 417, and 424 nm with approximate sizes of QDs 3.4, 3.58, 3.78, 3.96, and 4.22 nm (as calculated from equation 1), respectively. A shift in absorption spectra was observed with increasing growth time, indicating increased CdS QDs size for earlier samples [27].

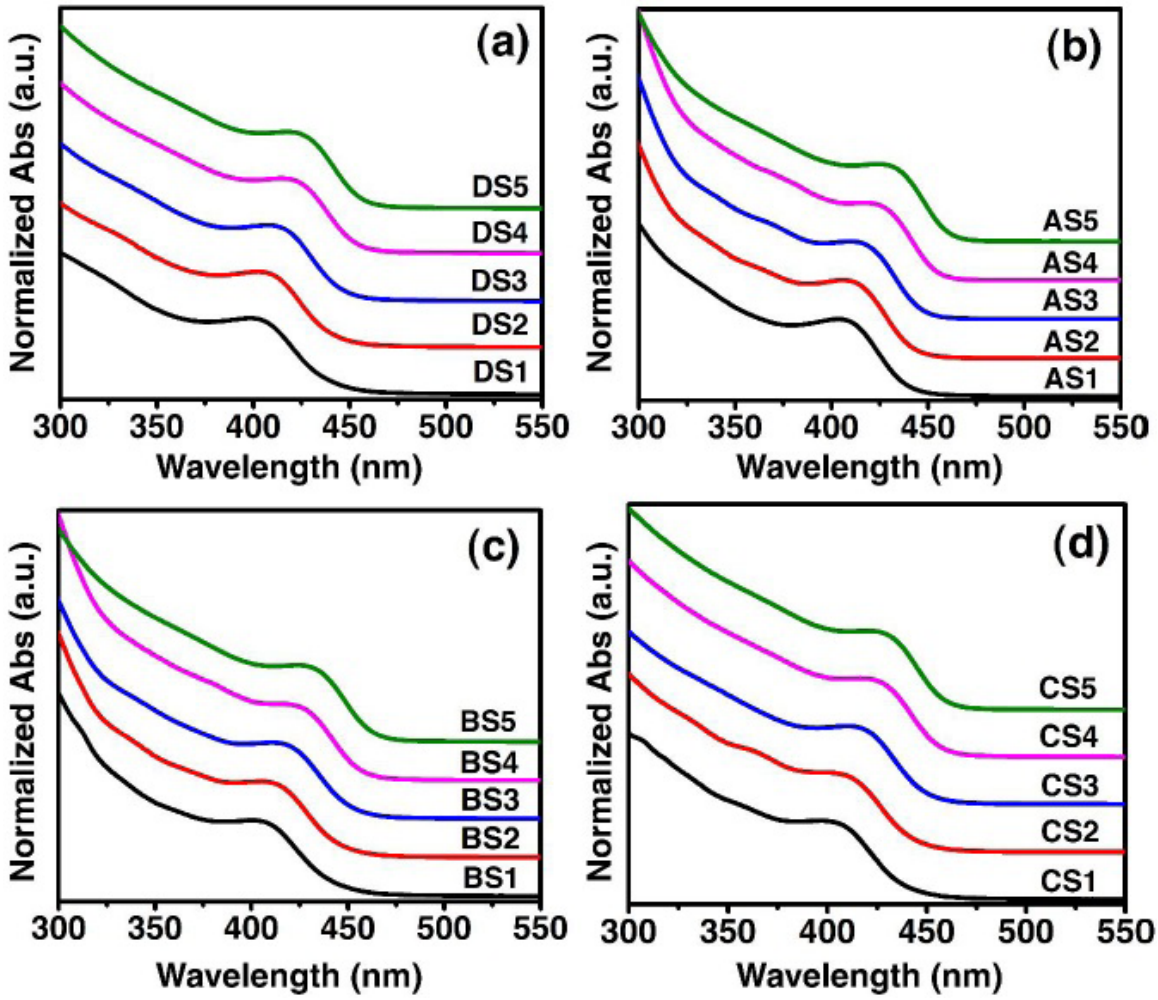

Figure 2. UV-Vis Absorption spectra of OA caped CdS with different OA concentration during reaction **(a)** 0 ml, **(b)** 1000 µl, **(c)** 500 µL and **(d)** 100 µL.

Similarly, Fig. 2(d) shows the absorption spectra of CdS QDs prepared under the same other condition with 100 µL OA. The absorption peaks at 400, 405, 410, 416, and 421 nm correspond to samples CS1, CS2, CS3, CS4, and CS5, respectively. The approximate sizes of QDs were 3.35, 3.5, 3.7, 3.9, and 4.1 nm as calculated using equation 1, respectively. Redshift occurred in the absorption spectra as growth time increased, indicating the increase in particle size and decrease in band gap from bulk CdS, thereby confirming the quantum confinement effect in the CdS QDs [27-28].

It has been observed that the average growth of QDs slowed after about 30 s because the initial nucleation of CdS QDs decreased considerably with decreasing initial OA concentration. When we increased the OA concentration in the reaction solution during the synthesis process, the initial Cd–oleate monomer concentration in the reaction mixture was increased. Further, these monomers acted as nuclei for nanocrystal growth of CdS QDs, leading to the faster growth rate of QDs. Therefore, by controlling the OA concentration, we can tune the size and absorption of CdS QDs.

The PL study is susceptible to the electronic structure of the QDs and very helpful in studying the effects of growth time on the emission properties of QDs. The present study obtained the PL spectra at room temperature at the excitation wavelength of 310 nm. Fig. S1(a) shows the emission spectra of DS1, DS2, DS3, DS4, and

DS5. Each of the colloidal solutions showed two emission peaks in the visible region. The first emission peaks were observed at 433, 438, 442, 451, and 453 nm for samples DS1, DS2, DS3, DS4, and DS5, respectively, indicating a redshift in the emission peak with reaction time (growth time), which is an indication of an increase in the size of QDs. Second broad emission peaks at a higher wavelength (> 500 nm) could be electron transitions from conduction band edge to surface states of the QD. The ligands and reaction times affect the size and PL properties, resulting in small peaks in the range of 375-400 nm [29].

The PL study was carried out to study the effect of OA concentration on emission properties of CdS QDs. Fig. S1(b-d) shows emission spectra of CdS QD prepared with 1000, 500, and 100 µL of OA. For example, the emission peaks were observed at 431, 433, 437, 445, and 452 nm corresponding to AS1, AS2, AS3, AS4, and AS5, respectively. Emission peaks were red-shifted in the emission spectra with growth time, indicating the increase in particle size with time. A broad peak was observed between 500 to 600 nm due to the presence of surface defects. These defects are trap states on which electrons were localized upon excitation and then showed a low energy emission *via* deep trap states or surface localized states recombination [30]. Defects present in QDs arise due to the presence of sulfur vacancies [31-32].

Fig. 3(a) shows the typical TEM image of the prepared sample DS3. The average size of QDs was between 3.5 to 4.0 nm, corresponding to the nanocrystal size obtained from the first excitonic peak of absorption spectra, as shown in Fig. 3(b). This also resembles the size of CdS QDs observed with the help of UV-Vis spectra and equation 1. The QDs tend to aggregate, as shown in Fig. 3(a).

It might happen due to less OA present in olive oil, which decreased viscosity and increased the chances of agglomeration. OA acts as a capping agent with steric hindrance around CdS QDs and suppresses the agglomeration of QDs. Fig. 3(c) shows the TEM image of sample BS3, which indicated that the size of QDs was ~3.7 nm. The size distribution of nanocrystal is shown in Fig. 3(d). Fig. 3(e) shows the TEM image of sample AS3, and the size distribution of the nanocrystal is shown in Fig. 3(f), indicating the size of the nanocrystal is also ~3.7 nm. It has been observed that with increasing the OA concentration, the dispersibility of QDs in toluene was increased due to steric hindrance. Furthermore, the OA is an efficient capping agent for synthesizing CdS QDs and tuning the optical properties with high dispersibility.

3.2 Ligand exchange reaction (Water dispersible QDs)

OA capped CdS QDs were dispersed in the non-polar solvent because of the long-chain hydrocarbon on the surface of QDs. At the same time, some applications require it as water-dispersible. We performed the ligand exchange reaction with sample BS3 to make the CdS QDs water-soluble. The OA was replaced by strong binding agent MPA, which has a thiol group (-SH) at one end and a carboxylic group (-COOH) at other end. According to the hard and soft acids and bases theory, the hard-hard or soft-soft molecules or ions can form a strong binding. The Cd^{2+} is classified as a soft ion and has a more robust interaction with the soft -SH group (from MPA) and low with –COOH (from OA). As a result, the -SH group can form a strong bond with CdS, and the other end has free carboxylic acid groups,

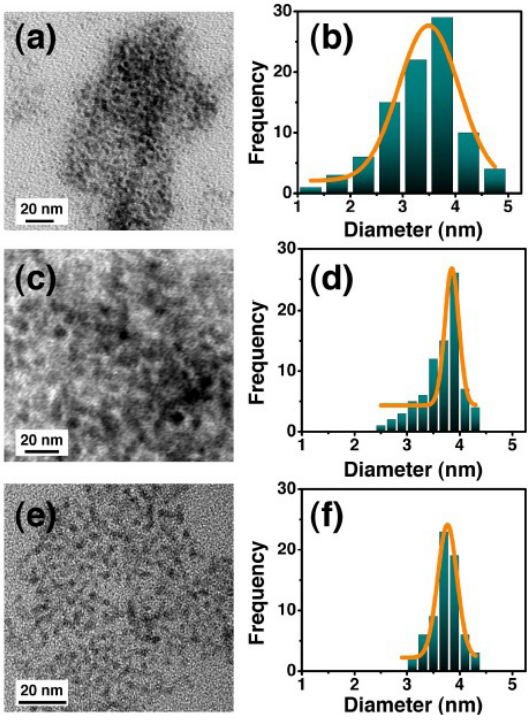

Figure 3. TEM image and size distribution of sample DS3 **(a, b)**, BS3 **(c, d)** and AS3 **(e, f)**.

which cause nanoparticles to be dispersible in polar solvents like DI water. Schematics of ligand exchange from OA capped CdS to MPA capped CdS is shown in Fig. 1. The effect of MPA capping on light absorption of CdS QDS has been studied by UV-Vis absorption (Fig. S2), showing a very little red shift.

3.3 FTIR study of MPA capped CdS

Fig. 4(a) shows a broad peak in the range of 3100–3000 cm^{-1}, which is owing to the C-H stretching vibration of alkyl group and –OH stretching vibration of –COOH group, while C-O stretching vibration occurred in the range of 1300 to 1000 cm^{-1} [15,33].The peak at 1704 cm^{-1} was occurred due to the stretching vibration of C=O for the MPA sample, while this peak is also present in the MPA capped CdS, owing to excess MPA present in the sample [34]. The peak at 1542 cm^{-1} occurred due to the COO^- band indicating the free carboxylic group in MPA capped CdS QDs [34]. The peaks observed at 2663 cm^{-1} and 2570 cm^{-1} in pure MPA were due to the S-H bond of the thiol group, which disappeared in MPA capped CdS sample, indicating the binding of the thiol group with CdS QDs [35]. The C-S vibration mode was assigned to the appearance of a peak at a lower wavenumber (662 cm^{-1}). The absorption band at 1396 cm^{-1} was due to the MPA's C–C single bond [36]. The FTIR spectra of pure OA and OA capped CdS QDs have been discussed in Supporting Information (Fig. S3).

3.4 TEM Image of MPA capped CdS

Fig. 4(b) shows TEM image of MPA-capped CdS QDs (BS3). The size distribution of QDs is shown in Fig. 4(c), indicating the average size of QDs was ~4 nm, which corresponds to the size obtained with the first excitonic peak of UV-Vis spectra of MPA capped CdS QDs.

The MPA-capped QDs are well distributed as compared with the OA-capped QDs. This might be because a long chain of OA has less steric repulsion than electro-repulsion by negatively charged carboxylic ions in MPA-capped CdS. The surface charges of MPA-capped CdS have been determined by Zeta potential (Fig. S4), showing a -12.86 mV charge on the surface of MPA-capped CdS QDs.

3.5 Effect of Ag-doping on CdS QDs

We studied the optical absorption, emission, crystal structure, lifetime of the created exciton, and surface morphology of Ag-doped CdS QDs with changes in the doping concentration. The UV-Vis absorption spectra were collected for the colloidal solutions of the different Ag-doped QDs, as shown in Fig. 5(a).

Fig. 5 (a) shows the absorption spectra of undoped CdS and Ag-doped CdS (Ag to Cd mole ratio equal to 0.6, 1.2, and 1.8%). The undoped CdS shows a characteristic absorption peak at 407 nm. Ag doped CdS QDs show absorption peaks at 408, 410, and 412 nm for samples with 0.6, 1.2 and 1.8% Ag doping, respectively. The result shows a significant redshift in the absorption spectra after Ag doping, which indicates the increased size of the Ag-doped CdS QDs upon Ag doping.

Fig. 5(b) shows emission spectra of Ag-doped CdS QDs with Ag to Cd molar ratios of 0.6, 1.2, and

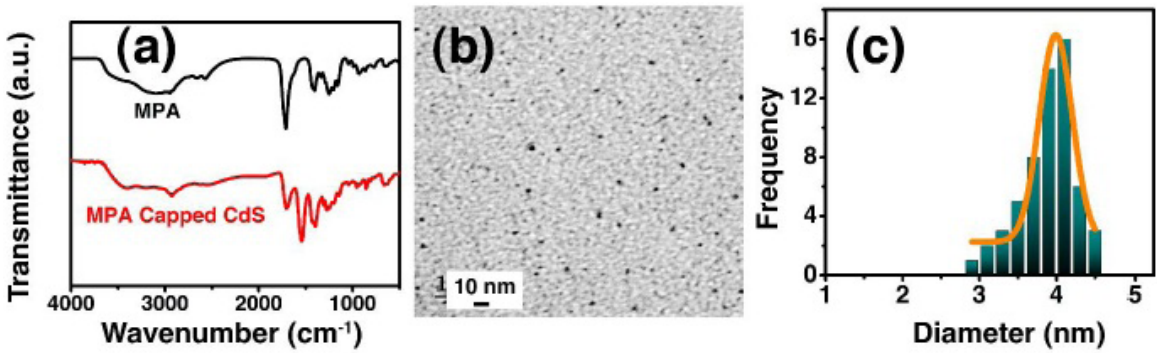

Figure 4. **(a)** FTIR spectra of pure MPA and CdS capped MPA, **(b)** TEM image of MPA-capped CdS QDs ligand exchange with sample BS3 **(a)** and **(c)** the nanoparticle size distribution of QDs.

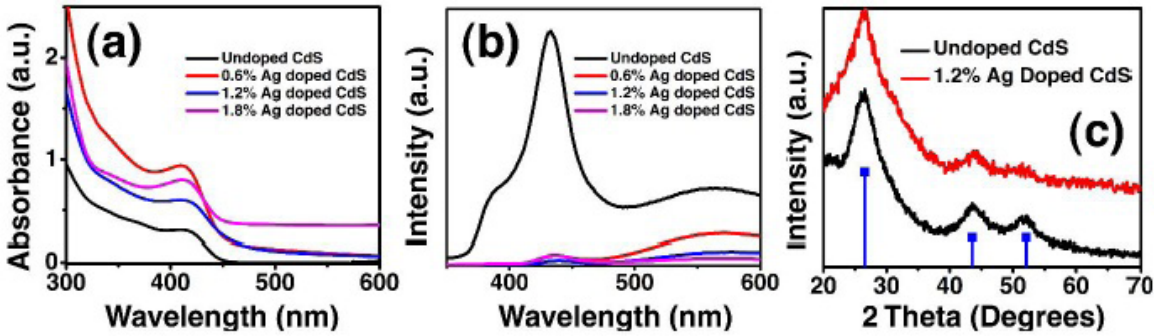

Figure 5. **(a)** UV-Vis absorption and **(b)** emission spectra of undoped CdS and Ag doped CdS QDs with [Ag]: [Cd] molar ratio 0.6. 1.2 and 1.8%, and **(c)** XRD spectra of undoped CdS QDs and Ag doped CdS QDs with 1.2% molar ratio of [Ag]/[Cd].

Sample	d_{002} (Å)	Lattice constant from d_{002} (Å)
CdS undoped	3.36	6.72
Ag doped CdS, Ag/Cd=1.2%	3.33	6.66

Table 1. Comparision of d value and lattice constants of CdS QDs before and after doping

1.8%. The emission peak at 390 nm corresponds to the band edge emission of the QDs. The emission peak at 434 nm was due to electron-hole recombination in the CdS QD. The Green emission at 567 nm was associated with the emission due to electronic transition from the conduction band to an acceptor level due to interstitial sulfur shallow trap emission. With the increase in the Ag doping concentration, the emission intensity of CdS was decreased. At higher Ag doping concentration, the emission intensity reduced drastically, suggesting a higher lifetime of excitons.

The electron and hole pairs were generated upon excitation under UV light. As the conduction band of CdS QDs was at a higher energy state than the work function of Ag, it facilitated the electron transfer between the CdS and the Ag metal. The higher Ag doping concentration results in higher interaction between CdS and Ag, and electron transfer was much faster than a lower Ag content which was observed with a decrease in the emission intensity.

3.6 XRD spectra of doped and undoped CdS QDs

Fig. 5(c) shows XRD spectra of undoped and Ag-doped CdS QDs with 1.2% [Ag]/[Cd] molar ratio. XRD spectra of undoped CdS QDs shows characteristics peaks at 26.52, 43.58 and 51.26° corresponding to planes at [111], [200], and [311], with d-values of 3.36, 2.07 and 1.78 Å, respectively (JCPDS: 89-0440). The doping with Ag resulted in overlapping peaks at 43.58 and 51.26°, which indicated that the hexagonal phase also existed [37]. Also, no extra peaks were observed in the spectra of 1.2% Ag doped CdS QDs, which belong to Ag alone, and Ag_2S did not form within the crystal structure. A small shift in angle was also observed in the sample of 1.2% Ag doped CdS QDs. The Ag doped CdS QDs showed peaks at 26.72, 43.77, and 51.46°, corresponding d-spacing values of 3.33, 2.06, and 1.77 Å, respectively. The decrease in the lattice constant with the doping is observed due to the replacement of Cd by Ag in the crystal structure [38-39]. Table 1 shows the comparison of d spacing and lattice constants of CdS QDs before and after doping.

3.7 TEM and TRPL analysis

We performed the TEM analysis to examine the effect of Ag doping on nanostructure morphology. Fig. 6(a) shows TEM images of collected aliquots of Ag-doped CdS QDs ([Ag]/[Cd]=1.2%) at the time interval of 5 min. The nanoparticles' sizes are 4-6 nm, with an average size of 5 nm (Fig. 6(b)). Fig. 6 (c) shows the absorption spectra of collected Ag-doped CdS QDs at 5 min intervals, showing peaks at 390 and 452 nm.

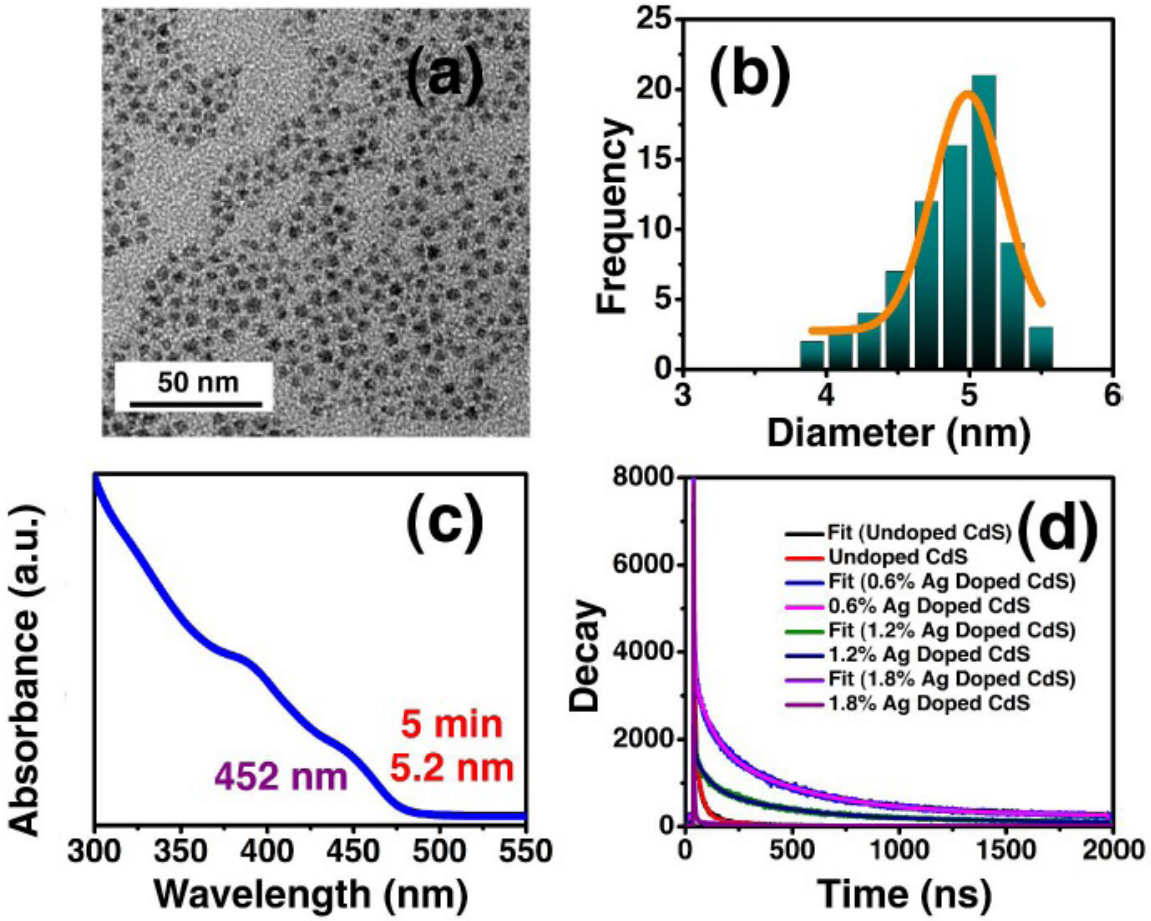

Figure 6. CdS QDs with [Ag]/[Cd] molar ratio 1.2% taken at 5 min **(a)** TEM image, **(b)** particle size distribution, **(c)** absorption spectra of 5 min sample, and **(d)** time resolve PL decay of undoped and Ag doped CdS QDs.

The lifetime of excitons in doped and undoped CdS was investigated by measuring the time-resolved PL decay (TRPL). We monitored the emission decay at 410 nm and fitted in three exponential kinetic programs. It consisted of 10-1000 ns time domains. The total average lifetime is obtained using equation 2.

$$\tau_{avg} = \frac{a_1\tau_1 + a_2\tau_2 + a_3\tau_3}{a_1 + a_2 + a_3} \quad [2]$$

where a_1, a_2 and a_3 denote the amplitude shallow, deeper, and deepest trap emissions, respectively. The decay components τ_1, τ_2, and τ_3 were considered due to the shallow, deeper, and deepest traps, respectively. The electrons present in the conduction band or shallow trap states of nanostructure are delocalized in nature [35]. As a result, there would be a significant electron and hole wave functions overlap. It also increases the electronic potential, causing the valence band position to shift, which is responsible for faster decay due to higher exciton recombination probability.

We know that the electrons and holes recombination on the QDs surface leads to surface-related emission [40]. For Ag-doped CdS QDs, Ag facilitates the trap formation for photoexcited electrons and holes. It results in the delay of the recombination process and significantly enhances the lifetime of excitons. Fig. 6(d) shows the TRPL decay comparison between undoped and Ag doped (0.6, 1.2, and 1.8%) CdS QDs.

At low doping concentration (0.6%), the increase in a lifetime was attributed to CdS/Ag complex formation compared to undoped CdS (Table 2). The exciton's average lifetime(s) was increased from 12 to 88.28 ns with the increase in the Ag

Lifetime value	CdS undoped (ns)	0.6% Ag doped CdS (ns)	1.2% Ag doped CdS (ns)	1.8% Ag doped CdS (ns)
τ_1	28.13	77.39	63.314	13.119
τ_2	184.26	435.25	438.49	316.275
τ_3	3.36	3.1	1.87	1.56
τ (average)	12	88.29	29.79	2.87

Table 2. Lifetime analysis of undoped and Ag-doped CdS QDs.

molar ratio from 0 to 0.6%. Further rise in Ag doping concentration decreases the average lifetime to 29.79 and 2.87 ns for 1.2 and 1.8% Ag doping in CdS QDs, respectively.

CdS has the bottom conduction band (BCB) and the top valance band (TVB) energy levels of ~-4.0 and ~-6.5 eV, respectively concerning vacuum.[41-42] Whereas Ag_n atomic cluster's energy level changes from -1.32 eV (n=1) to - 4.64 eV (n=∞, bulk phase) [43-44]. At a deficient concentration of Ag doping, the photogenerated electrons cannot transfer from BCB of CdS to Ag_n. It is because of the much higher energy level of Ag_n than BCB. As the concentration increases, the Ag_n energy level decreases and starts accepting photogenerated electrons. It results in efficient electron transfer from BCB of CdS to Ag. However, with the increase in the Ag concentration during the synthesis process, the formation of Ag clusters was increased. These clusters provided traps for photoexcited electrons and holes, which enhanced the recombination process; as a result, the lifetime of excitons was reduced at higher concentrations of Ag doping.

The more Ag incorporation causes more overlap of the hole wave function with the electron wave function. It thereby generates more trapping states within the energy gap. In the nanostructures, the region between the conduction band minimum and the highest level of the trapping band is always associated with optical transition routes. When we achieve a critical value of Ag dopant, the trapping energy band and valance band maximum (VBM) merges. Thus, the energy gap possesses more trapping states. Therefore, we make efficient electron-hole recombination along with a shorter lifetime. The bandgap decreases because a more substantial hole wave function overlap with the increase in Ag dopant. The synthesized materials can be for photocatalytic water splitting, solar cells, sensors, etc. [45-48].

4 Conclusions

We have successfully synthesized colloidal undoped and Ag-doped CdS QDs *via* a low-cost, green, and environment-friendly approach. Synthesized CdS QDs showed different optical properties with variations in size. The OA played a very significant role in controlling the size of QDs by steric hindrance. After ligand exchange, water dispersible CdS QDs were successfully synthesized. Also, CdS QDs were successfully doped with Ag to improve their optical properties. XRD and absorption/emission spectra confirmed Ag doping. The prepared QDs could find potential applications such as photocatalytic water splitting, dye sensitized solar cells, sensors, etc. Water dispersible CdS QDs can also be helpful for drug delivery, biosensing, and targeting cancer cell applications.

Acknowledgments

RKG acknowledges financial assistance from the Department of Science and Technology (DST), India INSPIRE Faculty Award (Project No. IFA-13 ENG-57) and Grant No. DST/TM/WTI/2K16/23(G).

Conflicts of interest

The authors declare no competing interest.

References

[1] Makvandi P, Ashrafizadeh M, Ghomi M, Najafi M, Hossein HHS, Zarrabi A, Mattoli V, Varma RS. Injectable hyaluronic acid-based antibacterial hydrogel adorned with biogenically synthesized AgNPs-decorated multi-walled carbon nanotubes. Prog Biomater. 2021;10(1):77-89.

[2] Xiang X, Zhu B, Cheng B, Yu J, Lv H. Enhanced photocatalytic H_2-production

activity of CdS quantum dots using Sn^{2+} as cocatalyst under visible light irradiation. Small. 2020;16(26):2001024.

[3] Duan L, Hu L, Guan X, Lin C-H, Chu D, Huang S, Liu X, Yuan J, Wu T. Quantum dots for photovoltaics: A tale of two materials. Adv Energy Mater. 2021;11(20):2100354.

[4] Bezinge L, Suea-Ngam A, deMello AJ, Shih C-J. Nanomaterials for molecular signal amplification in electrochemical nucleic acid biosensing: Recent advances and future prospects for point-of-care diagnostics. Mol Syst Des Eng. 2020; 5(1):49-66.

[5] Wang S, Yu J, Zhao P, Li J, Han S. Preparation and mechanism investigation of CdS quantum dots applied for copper ion rapid detection. J Alloys Compd. 2021;854(157195.

[6] Sonker RK, Shastri R, Johari R. Superficial synthesis of CdS quantum dots for an efficient perovskite-sensitized solar cell. Energy Fuels. 2021;35(9):8430-8435.

[7] Ren H-H, Fan Y, Wang B, Yu L-P. Polyethylenimine-capped CdS quantum dots for sensitive and selective detection of nitrite in vegetables and water. J Agric Food Chem. 2018;66(33):8851-8858.

[8] Wang F, Tang R, Kao JLF, Dingman SD, Buhro WE. Spectroscopic identification of tri-n-octylphosphine oxide (TOPO) impurities and elucidation of their roles in cadmium selenide quantum-wire growth. J Am Chem Soc. 2009;131(13):4983-4994.

[9] Shivaji K, Mani S, Ponmurugan P, De Castro CS, Lloyd Davies M, Balasubramanian MG, Pitchaimuthu S. Green-synthesis-derived CdS quantum dots using tea leaf extract: Antimicrobial, bioimaging, and therapeutic applications in lung cancer cells. ACS Appl Nano Mater. 2018;1(4):1683-1693.

[10] Moradi Alvand Z, Rajabi HR, Mirzaei A, Masoumiasl A, Sadatfaraji H. Rapid and green synthesis of cadmium telluride quantum dots with low toxicity based on a plant-mediated approach after microwave and ultrasonic assisted extraction: Synthesis, characterization, biological potentials and comparison study. Mater Sci Eng, C. 2019;98(535-544.

[11] Makvandi P, Baghbantaraghdari Z, Zhou W, Zhang Y, Manchanda R, Agarwal T, Wu A, Maiti TK, Varma RS, Smith BR. Gum polysaccharide/nanometal hybrid biocomposites in cancer diagnosis and therapy. Biotechnol Adv. 2021;48(107711.

[12] Makvandi P, Ghomi M, Padil VVT, Shalchy F, Ashrafizadeh M, Askarinejad S, Pourreza N, Zarrabi A, Nazarzadeh Zare E, Kooti M, Mokhtari B, Borzacchiello A, Tay FR. Biofabricated nanostructures and their composites in regenerative medicine. ACS Appl Nano Mater. 2020;3(7): 6210-6238.

[13] Pu Y, Cai F, Wang D, Wang J-X, Chen J-F. Colloidal synthesis of semiconductor quantum dots toward large-scale production: A review. Ind Eng Chem Res. 2018; 57(6):1790-1802.

[14] Jouyandeh M, Mousavi Khadem SS, Habibzadeh S, Esmaeili A, Abida O, Vatanpour V, Rabiee N, Bagherzadeh M, Iravani S, Reza Saeb M, Varma RS. Quantum dots for photocatalysis: Synthesis and environmental applications. Green Chem. 2021;23(14):4931-4954.

[15] Bel Haj Mohamed N, Ben Brahim N, Mrad R, Haouari M, Ben Chaâbane R, Negrerie M. Use of MPA-capped CdS quantum dots for sensitive detection and quantification of Co^{2+} ions in aqueous solution. Anal Chim Acta. 2018;1028(50-58.

[16] Veerathangam K, Pandian MS, Ramasamy P. Size-dependent photovoltaic performance of cadmium sulfide (CdS) quantum dots for solar cell applications. J Alloys Compd. 2018;735(202-208.

[17] Singh N, Mondal K, Misra M, Sharma A, Gupta RK. Quantum dot sensitized electrospun mesoporous titanium dioxide hollow nanofibers for photocatalytic applications. RSC Adv. 2016;6(53):48109-48119.

[18] D RD, S N, R R, T S. Green synthesis of CdS quantum dot using (Citrus Limon (L.) Osbeck) leaves extract as stabilizing agent and investigate its emission properties. Mater Today: Proc. 2021.

[19] Kim D, Gu M, Park M, Kim T, Kim B-S. Layer-by-layer assembly for photoelectrochemical nanoarchitectonics. Mol Syst Des Eng. 2019;4(1):65-77.

[20] Kyobe JW, Mubofu EB, Makame YMM, Mlowe S, Revaprasadu N. Cadmium sulfide quantum dots stabilized by

castor oil and ricinoleic acid. Physica E. 2016;76(95-102.
[21] Kyobe JW, Mubofu EB, Makame YMM, Mlowe S, Revaprasadu N. CdSe quantum dots capped with naturally occurring biobased oils. New J Chem. 2015;39(9): 7251-7259.
[22] Yang Z, Lu L, Berard VF, He Q, Kiely CJ, Berger BW, McIntosh S. Biomanufacturing of CdS quantum dots. Green Chem. 2015;17(7):3775-3782.
[23] Kandasamy K, Venkatesh M, Syed Khadar YA, Rajasingh P. One-pot green synthesis of CdS quantum dots using Opuntia ficus-indica fruit sap. Mater Today: Proc. 2020;26(3503-3506.
[24] Maity P, Kumar S, Kumar R, Jha SN, Bhattacharyya D, Barman SR, Chatterjee S, Pal BN, Ghosh AK. Role of cobalt doping in CdS quantum dots for potential application in thin film optoelectronic devices. J Phys Chem C. 2021;125(3):2074-2088.
[25] Butwong N, Srijaranai S, Luong JHT. Fluorometric determination of hydrogen sulfide via silver-doped CdS quantum dots in solution and in a test strip. Microchim Acta. 2016;183(3):1243-1249.
[26] Thakur P, Joshi SS, Kapoor S, Mukherjee T. Fluorescence behavior of cysteine-mediated Ag@CdS nanocolloids. Langmuir. 2009; 25(11):6377-6384.
[27] Yu WW, Qu L, Guo W, Peng X. Experimental determination of the extinction coefficient of CdTe, CdSe, and CdS nanocrystals. Chem Mater. 2003;15(14):2854-2860.
[28] Bansal AK, Antolini F, Zhang S, Stroea L, Ortolani L, Lanzi M, Serra E, Allard S, Scherf U, Samuel IDW. Highly luminescent colloidal CdS quantum dots with efficient near-infrared electroluminescence in light-emitting diodes. J Phys Chem C. 2016;120(3):1871-1880.
[29] Deng Z, Lie FL, Shen S, Ghosh I, Mansuripur M, Muscat AJ. Water-based route to ligand-selective synthesis of ZnSe and Cd-doped ZnSe quantum dots with tunable ultraviolet A to blue photoluminescence. Langmuir. 2009; 25(1):434-442.
[30] Kumar N, Alam F, Dutta V. Photoluminescence study of oleic acid capped and hexanoic acid washed CdS quantum dots. RSC Adv. 2016;6(34):28316-28321.
[31] Trindade T, O'Brien P, Pickett NL. Nanocrystalline semiconductors: Synthesis, properties, and perspectives. Chem Mater. 2001;13(11):3843-3858.
[32] Ganiga M, Cyriac J. An ascorbic acid sensor based on cadmium sulphide quantum dots. Anal Bioanal Chem. 2016;408(14): 3699-3706.
[33] Liu X, Na W, Qu Z, Su X. Turn-off–on fluorescence probe based on 3-Mercaptopropionic acid-capped CdS quantum dots for selective and sensitive lysozyme detection. RSC Adv. 2016;6(89):85795-85801.
[34] Jiménez-Hernández L, Estévez-Hernández O, Hernández-Sánchez M, Díaz JA, Farías- Sánchez M, Reguera E. 3-Mercaptopropionic acid surface modification of Cu-doped ZnO nanoparticles: Their properties and peroxidase conjugation. Colloids Surf, A. 2016;489(351-359.
[35] Tang J, Kemp KW, Hoogland S, Jeong KS, Liu H, Levina L, Furukawa M, Wang X, Debnath R, Cha D, Chou KW, Fischer A, Amassian A, Asbury JB, Sargent EH. Colloidal-quantum-dot photovoltaics using atomic-ligand passivation. Nat Mater. 2011;10(10):765-771.
[36] Bel Haj Mohamed N, Haouari M, Zaaboub Z, Hassen F, Maaref H, Ben Ouada H. Effect of surface on the optical structure and thermal properties of organically capped CdS nanoparticles. J Phys Chem Solids. 2014;75(8):936-944.
[37] Yousefi M, Abdolhosseinzadeh A, Fallah H, Khosravi A. Growth and characterization of CdS and CdS: Ag luminescent quantum dots dispersed in solution. Mod Phys Lett B. 2010;24(25):2591-2599.
[38] Bakhsh EM, Khan MI. Clove oil-mediated green synthesis of silver-doped cadmium sulfide and their photocatalytic degradation activity. Inorg Chem Commun. 2022;109256.
[39] Iqbal T, Ara G, Khalid NR, Ijaz M. Simple synthesis of Ag-doped CdS nanostructure material with excellent properties. Appl Nanosci. 2020;10(1):23-28.
[40] Munishwar SR, Pawar PP, Janbandhu SY, Gedam RS. Highly stable CdS quantum

dots embedded in glasses and its application for inhibition of bacterial colonies. Opt. Mater. 2020;99(109590.

[41] Ma X-C, Dai Y, Yu L, Huang B-B. Energy transfer in plasmonic photocatalytic composites. Light Sci Appl. 2016;5(2): e16017-e16017.

[42] Li J, Wu N. Semiconductor-based photocatalysts and photoelectrochemical cells for solar fuel generation: a review. Catal Sci Technol. 2015;5(3):1360-1384.

[43] Bae G-T, Aikens CM. Time-dependent density functional theory studies of optical properties of Ag nanoparticles: Octahedra, truncated octahedra, and icosahedra. J Phys Chem C. 2012;116(18):10356-10367.

[44] Makkar P, Ghosh NN. A review on the use of DFT for the prediction of the properties of nanomaterials. RSC Adv. 2021;11(45):27897-27924.

[45] Veerathangam K, Pandian MS, P R. Photovoltaic performance of Ag-doped CdS quantum dots for solar cell application. Mater Res Bull. 2017;94(371-377.

[46] Rabizadeh H, Feizbakhsh A, Ahmad Panahi H, Konoz E. Synthesis and characterization of Ag doped cadmium sulfide/multi walled carbon nanotubes: Structural, and photocatalysis studies. Fuller Nanotub Carbon Nanostructures. 2019;27(10):788-795.

[47] Butwong N, Kunthadong P, Soisungnoen P, Chotichayapong C, Srijaranai S, Luong JHT. Silver-doped CdS quantum dots incorporated into chitosan-coated cellulose as a colorimetric paper test stripe for mercury. Microchim Acta. 2018; 185(2):126.

[48] Boxi SS, Paria S. Fluorometric selective detection of fluoride ions in aqueous media using Ag doped CdS/ZnS core/ shell nanoparticles. Dalton Trans. 2016; 45(2):811-819.

Supplementary

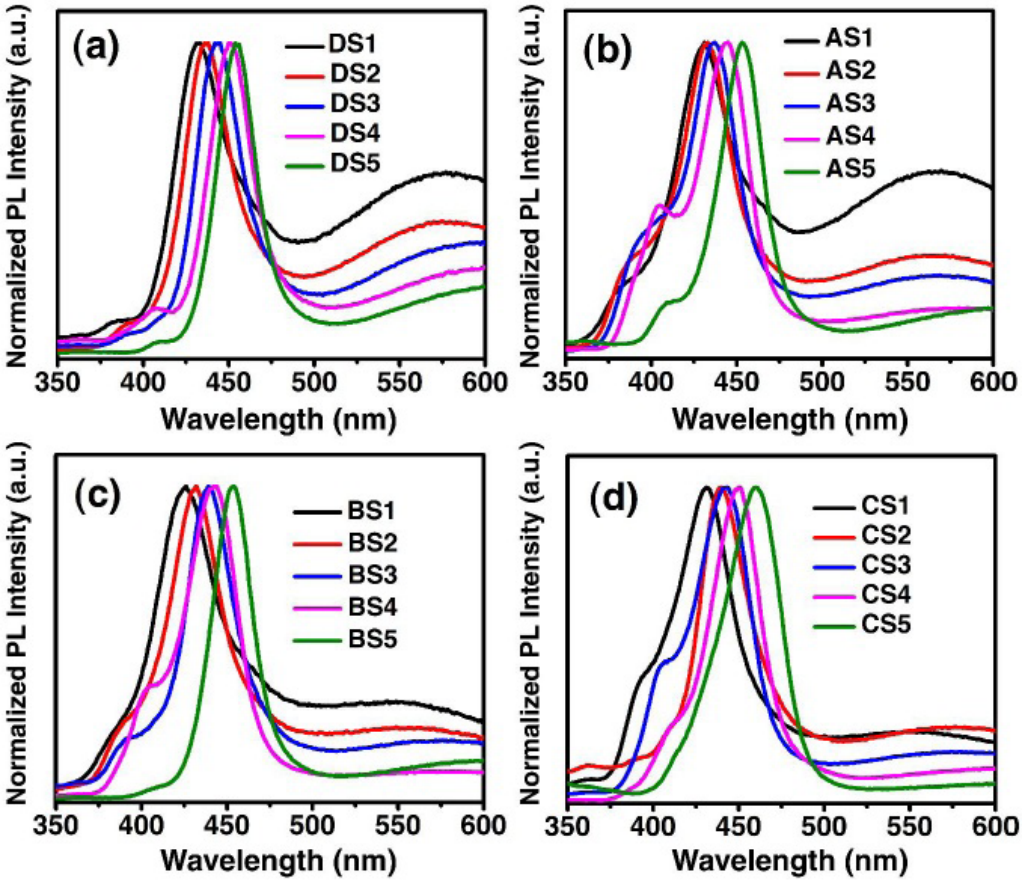

Figure S1. Emission spectra of OA capped CdS with different OA amount in reaction (a) 0 ml, (b) 1000 µl, (c) 500 µL and (d) 100 µL.

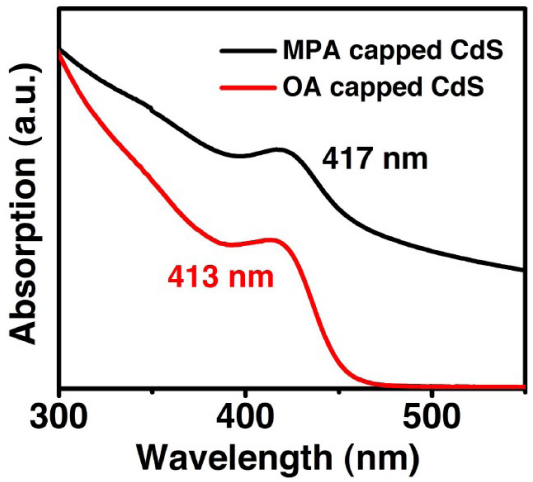

Figure S2. Absorption spectra of OA capped and MPA capped CdS QDs.

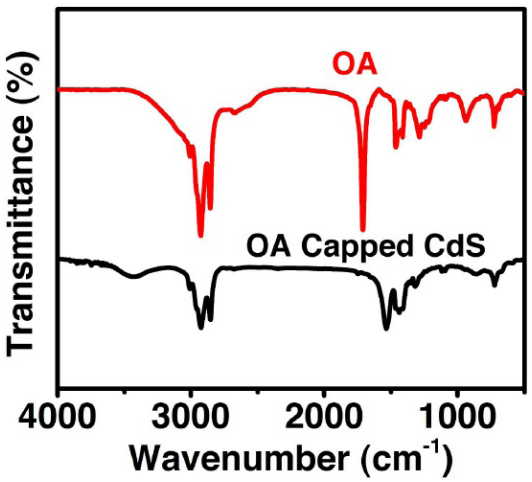

Figure S3. FTIR spectra of pure OA and OA capped CdS QDs.

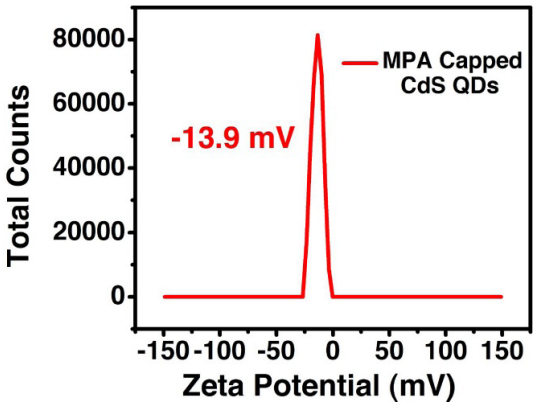

Figure S4. Zeta potential of MPA capped CdS QDs.